# Mechanistic Complexity of Methane Oxidation with $H_2O_2$ by Single-Site Fe/ZSM-5 Catalyst

Szécsényi, Ágnes; Li, Guanna; Gascon, Jorge; Pidko, Evgeny A.

**DOI**
10.1021/acscatal.8b01672

**Publication date**
2018

**Document Version**
Final published version

**Published in**
ACS Catalysis

ACS Catalysis

Research Article

Cite This: ACS Catal. 2018, 8, 7961−7972

pubs.acs.org/acscatalysis

# Mechanistic Complexity of Methane Oxidation with $H_2O_2$ by Single-Site Fe/ZSM-5 Catalyst

Ágnes Szécsényi,[†,‡,§] Guanna Li,[†,‡] Jorge Gascon,[§] and Evgeny A. Pidko*[,‡,∥]

[†]Catalysis Engineering Group, Chemical Engineering Department, and [‡]Inorganic Systems Engineering Group, Chemical Engineering Department, Delft University of Technology, Van der Maasweg 9, 2629 HZ Delft, The Netherlands

[§]Catalysis Center, Advanced Catalytic Materials, King Abdullah University of Science and Technology, Thuwal 23955, Saudi Arabia

[∥]TheoMAT Group, ITMO University, Lomonosova Street 9, St. Petersburg 191002, Russia

Supporting Information

**ABSTRACT:** Periodic density functional theory (DFT) calculations were carried out to investigate the mechanism of methane oxidation with $H_2O_2$ over the defined Fe sites in Fe/ZSM-5 zeolite. The initial Fe site is modeled as a $[(H_2O)_2{-}Fe(III){-}(\mu O)_2{-}Fe(III){-}(H_2O)_2]^{2+}$ extraframework cluster deposited in the zeolite pore and charge-compensated by two anionic lattice sites. The activation of this cluster with $H_2O_2$ gives rise to the formation of a variety of Fe(III)-oxo and Fe(IV)-oxo complexes potentially reactive toward methane dissociation. These sites are all able to promote the first C−H bond cleavage in methane by following three possible reaction mechanisms: namely, (a) heterolytic and (b) homolytic methane dissociation as well as (c) Fenton-type reaction involving free OH radicals as the catalytic species. The C−H activation step is followed by formation of MeOH and MeOOH and regeneration of the active site. The Fenton-type path is found to proceed with the lowest activation barrier. Although the barriers for the alternative heterolytic and homolytic pathways are found to be somewhat higher, they are still quite favorable and are expected to be feasible under reaction conditions, resulting ultimately in MeOH and MeOOH products. $H_2O_2$ oxidant competes with $CH_4$ substrate for the same sites. Since the oxidation of $H_2O_2$ to $O_2$ and two $[H^+]$ is energetically more favorable than the C−H oxofunctionalization, the overall efficiency of the latter target process remains low.

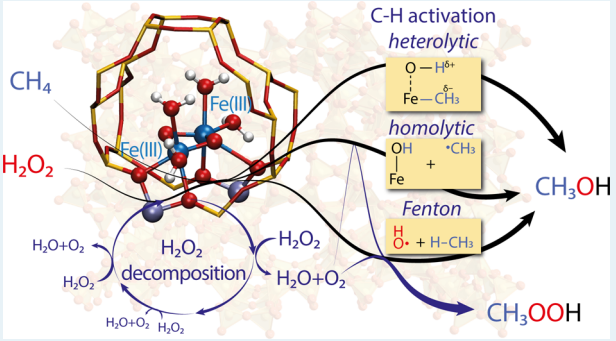


**KEYWORDS:** *selective oxidation, catalytic reaction networks, DFT calculations, zeolites, heterogeneous catalysis, computational chemistry, selectivity control*

## 1. INTRODUCTION

The conversion of methane to methanol is considered one of the greatest challenges in catalysis today.[1−3] Currently, a two-step process via synthesis gas is used in industry. For economic reasons, a one-pot production of methanol at near-ambient conditions is desirable.[4,5] The main challenge of this reaction is the targeted dissociation of the first C−H bond followed by formation of methanol, which is not the thermodynamically most stable oxidation product. It is easily converted further to other oxygenated hydrocarbons and carbon oxides. In the past hundred years, a tremendous amount of experimental and theoretical work on this process has been conducted.[3,6−8] Although the field had witnessed significant achievements, no direct methane oxofunctionalization process suitable for industrial implementation has been delivered so far.

The simplest alternative to the current two-step process is the thermal oxidation of methane.[9] Relatively high yields of oxygenated products can be achieved: 60% methanol selectivity at 12−13% methane conversion has been reported. Interestingly, it was proposed that the metal wall of the actual reactor is key to the low selectivity of the process, as it provides the catalytic sites for the overoxidation of methanol to carbon oxides. Although the methanol yields achieved by the thermal oxidation are quite impressive, it was concluded that no further improvement of the process could be delivered by optimization of operational conditions. The introduction of a catalyst capable of shifting selectivity away from the overoxidation path is necessary.[5]

Among the lower-temperature catalytic paths for methane oxofunctionalization, the catalytic system of Periana et al.[10,11] stands out as the most successful. It utilizes (bpym)Pt(II)$Cl_2$ homogeneous catalyst in concentrated sulfuric acid solvent at 200 °C, providing up to 81% selectivity to a methyl sulfate oxofunctionalization product at about 90% methane conversion. Despite its outstanding performance, this system is industrially

Received: April 28, 2018
Revised: July 10, 2018
Published: July 18, 2018






DOI: 10.1021/acscatal.8b01672
ACS Catal. 2018, 8, 7961−7972

not applicable due to the harsh reaction conditions and relatively low productivity.

In the past two decades, transition and nontransition metal clusters, such as Co, Fe, Cu, or Zn deposited in zeolites,[12−20] came to the forefront of catalytic oxidation research. Mainly three oxidizing agents were applied in combination with these catalysts: (1) $O_2$,[12,14] (2) $N_2O$[18,19] in gas−solid-phase reactions, and (3) $H_2O_2$[16,17] in liquid−gas-phase reactions. The greatest problem with gas−solid-phase reactions is that they are semicatalytic. Catalyst oxidation, methane activation, and methanol formation by hydrolysis of the strongly adsorbed methoxo species are carried out in separate process stages. Additionally, the product is obtained as a very low-concentration solution, which entails further costs of separation. Recently, promising improvements were achieved by the cofeeding of water in the reaction mixture.[21] An alternative solution is the liquid-phase reaction, where methane oxidation with liquid oxidants can be carried out in a single catalytic process. Among different systems considered, promising results were demonstrated by Hutchings and Hammond and their co-workers[16,17,22−24], who investigated the oxidation of methane to methanol over an iron-modified (Fe/ZSM-5) zeolite-based catalyst with $H_2O_2$ as the oxidant.

Understanding the nature of the catalytic species and reaction mechanism is key to rational optimization and improvement of heterogeneous catalyst. Extraframework clusters present in metal-exchanged zeolites can have different chemical composition and be located at different positions. Distinct configurations and clusters might have different catalytic activity and contribute differently to the overall selectivity of the catalytic process.[25−30] That is why a great deal of research has so far been devoted to discriminating the active site from the spectator species and identifying the reaction mechanism in zeolite catalysis. Panov and co-workers[18,19] have proposed that when $N_2O$ is used as the oxidant, the catalytic species providing a high reactivity of Fe/ZSM-5 toward C−H activation is Fe(IV)═O, denoted as the $\alpha$-oxygen. Later studies by Schoonheydt, Sels, Solomon, and co-workers[31,32] provided additional experimental evidence to this assignment and identified such mononuclear species as the active site for gas-phase methane oxofunctionalization.

These experimental findings are in line with earlier computational studies on the nature of catalytic sites for benzene oxidation with $N_2O$ by Fe/ZSM-5.[33] Li et al.[34] carried out a comprehensive study on the stability and reactivity of different Fe-containing species in ZSM-5 zeolite. It was found that isolated $Fe^{2+}$ species capable of forming the reactive $\alpha$-oxygen sites can only be formed within a small fraction of cationic sites featuring a symmetric arrangement of lattice Al sites. Most of the extraframework positions were proposed to be occupied by the alternative oxygen-bridged iron clusters. Importantly, only the isolated sites were shown to contribute to the catalytic benzene oxidation process, as C−H activation over the other species yields highly stable surface structures that effectively deactivate the respective Fe site.

Very recently, Nørskov and co-workers[35] reported a computational analysis of a wide range of materials for their ability to active C−H bonds in methane via a homolytic reaction mechanism (Scheme 1, pathway 2). In another example, researchers found that, in a $[Cu_3O_3]^{2+}$ cluster deposited in the zeolite framework, the O atom with higher spin density is more reactive.[36] In other cases, the authors compared clusters containing different metal ions. One study concluded that Ni is the best-performing among Cu, Zn, and Ni in homogeneous catalysts;[37] another study found that Cu is the best among Ni, Co, Fe, Ag, and Au when these metals are deposited in a ZSM-5 zeolite framework.[38]

**Scheme 1. Potential Mechanistic Pathways for C−H Bond Cleavage: (1) Heterolytic, (2) Homolytic, and (3) Fenton-type Activation Investigated in This Paper**

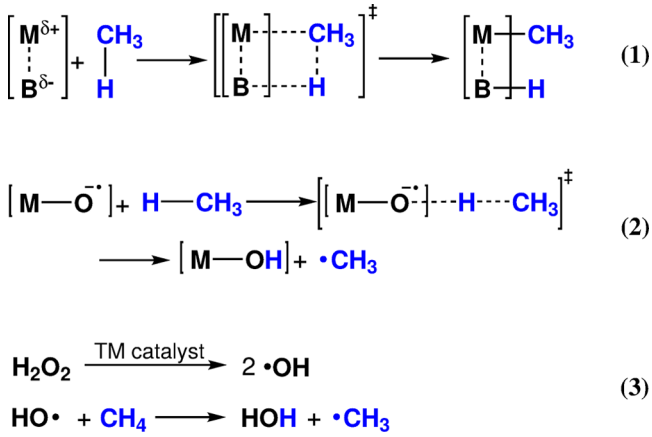


Two principal C−H activation mechanisms providing a path toward selective methane activation are usually distinguished: (1) heterolytic and (2) homolytic reaction mechanisms (Scheme 1).[39,40] In the former case, the C−H bond is activated over an acid−base pair to form an anionic alkyl group stabilized by the acid (often a metal cation) and a proton is accepted by the base part of the active site. Note that the heterolytic C−H cleavage is not accompanied by any redox processes within the active site. The actual oxidation of the alkyl moiety should then take place in subsequent steps of the overall catalytic process. In the homolytic mechanism, the C−H bond breaks with the formation of two radical species: the alkyl radical and a formally H radical. The H radical represents a transient species that is readily accepted by the basic moiety of the active site, which is at the same time reduced with 1 $e^-$. The subsequent rebound of the $CH_3$ radical completes the two-electron reduction process and yields the oxidized organic product or surface-bound intermediate. Given the fact that homolytic C−H activation commonly yield a free alkyl radical while the energy losses due to cleavage of a strong C−H bond come predominantly from single-electron reduction of the active complex accompanied by its protonation, the basicity of the proton-accepting site (B) (that is, basically, the strength of the resulting B−H bond) has been recognized as one of the critical parameters defining the overall reactivity of a catalyst toward homolytic C−H activation.[35,41] The direct relationships between this parameter and the computed barriers for C-H activation have been demonstrated in recent study by Nørskov and co-workers[42] for a wide class of potential heterogeneous catalysts.

In the chemistry of iron (see Plietker),[43] the preference for a particular C−H activation mechanism is usually defined by the oxidation state of the Fe site, its coordination environment, and the nature of the ligands.[39] Heterolytic C−H cleavage (Scheme 1, pathway 1) is commonly observed over the lower-valent Fe sites (e.g., 3+ and 2+) conjugated with a strong base site. The homolytic C−H dissociation (Scheme 1, pathway 2) is more typical for higher-valent Fe sites that feature more covalent-type bonding and facilitate the oxidative activation of the substrate coupled with the reduction of Fe. In addition to these two very generic reaction channels, scientists distinguish one more



DOI: 10.1021/acscatal.8b01672
ACS Catal. 2018, 8, 7961−7972

mechanism specific to Fe chemistry: that is, the Fenton-type mechanism of C−H activation (Scheme 1, pathway 3). Although formally this mechanism can be regarded as a subtype of the homolytic C−H bond dissociation (pathway 2), it is commonly considered separately in view of the secondary role the Fe site plays in it. In Fenton chemistry, iron ions initiate the radical oxidation paths by producing free OH radical species, which activate C−H bonds.[44,45] In the context of selective methane oxofunctionalization, Fenton-type reactions have been explored in works by Shulpin and co-workers[46−48] who demonstrated that, in the presence of Fe(II) ions, methane can be oxidized with $H_2O_2$ and $O_2$ to produce MeOOH as the main product. Similar chemistry has recently been proposed by Hutchings and co-workers[49] to govern methane oxidation by Pd nanoparticles.

In many cases, only one type of activation is investigated. For example, the structure−activity relationship derived by Nørskov and co-workers[35] is valid only under the assumption of homolytic C−H bond activation. However, there are density functional theory (DFT) studies that propose heterolytic methane dissociation over Cu and Fe clusters deposited in zeolites.[50−52] In a complex system such as transition-metal-exchanged zeolites, different clusters can be found,[34] which might promote diverse types of C−H bond activation. In our work, we aim to investigate how different Fe clusters influence the type and energetics of C−H bond cleavage. For this, we analyzed this reaction step over numerous clusters created from binuclear Fe(III)-oxo with $H_2O_2$ based on the catalytic system of Hutchings and co-workers.[16] Mostly theoretical work focuses on the rate-determining C−H bond activation step, but here we also present the whole catalytic cycle, including formation of the active site, C−H bond activation, and product formation followed by regeneration of the initial site. All three previously introduced potential reaction mechanisms were considered for methane activation. Comprehensive description of the reaction network provides us with atomic-level insights into this immensely complicated heterogeneous catalytic process.

## 2. MODEL AND SIMULATION DETAILS

The spin-polarized periodic DFT calculations were carried out with the Vienna ab initio simulation package (VASP).[53−56] The Perdew−Burke−Ernzerhof (PBE) exchange−correlation functional[57,58] was used together with a plane-wave basis set with a cutoff energy of 450 eV and the projector augmented wave (PAW) method.[59,60] To account for the van der Waals interactions, the semiempirical Grimme's dispersion correction with Becke−Jonson damping [DFT-D3(BJ)] method[61] was used. A Gaussian smearing of the population of partial occupancies with a width of 0.05 eV was used during iterative diagonalization of the Kohn−Sham Hamiltonian. Brillouin zone sampling was restricted to the Γ point.[62] Convergence was assumed to be reached when the force on each atom was below 0.04 eV·Å$^{-1}$.

To locate transition states, the nudged elastic band method (NEB)[63] was applied. The maximum energy geometry along the reaction path generated by the NEB method was further optimized by use of a quasi-Newton algorithm. In this procedure, only the extraframework atoms, and relevant framework atoms were relaxed. Vibrational frequencies were calculated by the finite difference method (0.02 Å atomic displacements) as implemented in VASP. Transition state showed a single imaginary frequency corresponding to the reaction path.

As an initial active-site model, a binuclear Fe cluster coordinated by framework oxygen atoms and extraframework $\mu$-oxo and water molecules at its first coordination shell with a total coordination number of 6 for each iron center (octahedral environment), $[(H_2O)_2{-}Fe(III){-}(\mu O)_2{-}Fe(III){-}(H_2O)_2]^{2+}$, is taken into consideration. The cluster is placed over the eight-membered ring of the zeolite. Two Si atoms of the ring are substituted with Al in the T7 and T12 sites (Figure 1). The unit

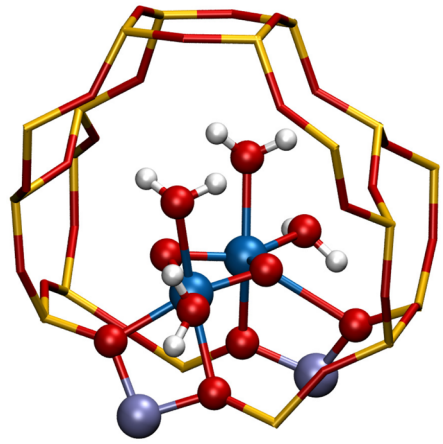

**Figure 1.** Initial $[(H_2O)_2{-}Fe(III){-}(\mu O)_2{-}Fe(III){-}(H_2O)_2]^{2+}$ model placed in the ZSM5 zeolite pore. The rest of the atoms in the periodic unit cell are omitted from the picture for the sake of visual clarity. Color code: Si, yellow; Al, purple; Fe, blue; O, red; H, white.

cell lattice parameters are optimized and are fixed throughout the calculations ($a = 20.1$, $b = 19.8$, $c = 13.2$, $\alpha = \beta = \gamma = 90°$). We based our assumption or the initial site on the DFT study of Li et al.,[34] which indicates this cluster as the most stable one among mono-, bi-, and tetranuclear species containing Fe(II) and Fe(III) ions in an oxidative aqueous environment. This is in agreement with the experimental and computational results of Hutchings and co-workers,[16] who concluded with high uncertainty an $[(H_2O)(HO){-}Fe{-}(\mu OH)_2{-}Fe{-}(OH){-}(H_2O)]^{2+}$ cluster as the representative species of their system. This cluster can be obtained from the previously described one by two $H^+$ transfers from the $H_2O$ molecules to the bridging O atoms, which is a very facile reaction, and does not change the stability of the cluster significantly, as we demonstrate in our calculations.

The octahedral environment may change during the course of the reaction; for example, one or both Fe atoms decoordinate from one of the framework O atoms. Due to the high number of structures, this is not elaborated in the text. Interested readers are invited to look at the files containing the geometry of each structure in Supporting Information.

All possible spin states ($S$ = 0−5) were considered for the initial Fe cluster. DFT calculations point to the $S = 3$ state as the most stable one. However, in this state one $H_2O$ molecule decoordinates from the Fe and forms a H bond with another $H_2O$ molecule, thus providing an artificial stabilization to the overall system. The release of $H_2O$ is triggered by the change of spin state, which results in different orbital energies, a change of ligand field, and therefore a change in the preferred geometry of the Fe complex. A similar effect is observed for the $S = 4$ state. The second most stable configuration is the antiferromagnetically coupled $S = 0$ state (broken symmetry singlet). Spin density analysis shows that the absolute value of spin assigned to each



DOI: 10.1021/acscatal.8b01672
ACS Catal. 2018, 8, 7961−7972

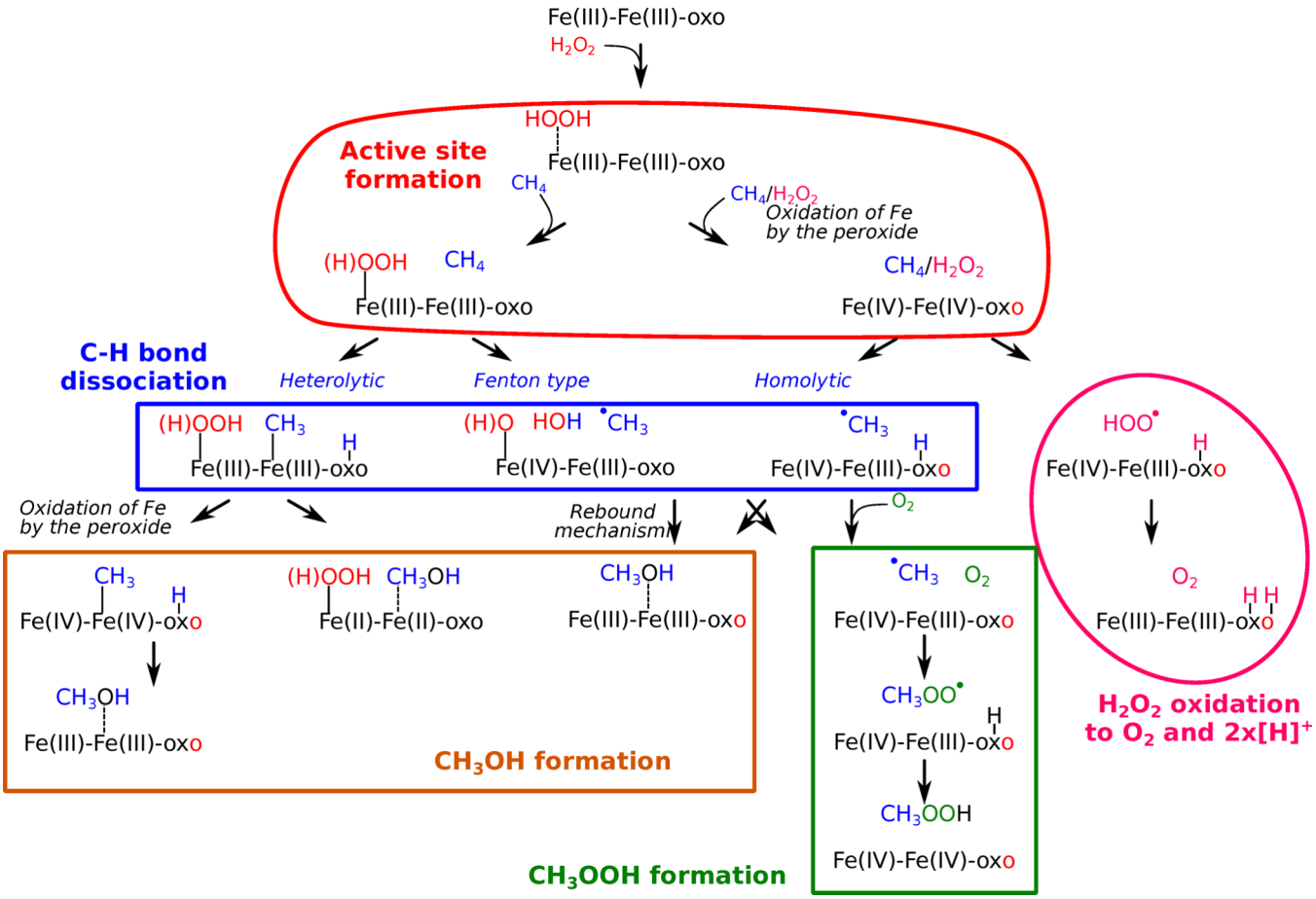


**Figure 2.** Schematic representation of the reaction network and most important steps underlying the oxidation of methane with $H_2O_2$ over Fe/ZSM-5 zeolite. Detailed descriptions of the structures can be found in Supporting Information.

atom is similar to those in the $S$ = 5 state. As it was shown previously that antiferromagnetic coupling does not significantly influence the reactivity in the case of O-bridged Fe dimers,[64] for the reactivity analysis we focused on the ferromagnetically coupled high-spin electronic configurations rather than the antiferromagnetically coupled $S$ = 0 state. Extensive justification for this simplification has been provided by Baerends and co-workers.[65] The preferred high- spin state changes over the course of the reaction with the oxidation state of the Fe cluster and the formation of radicals.

In this study, we base our mechanistic analysis on the discussion of relative electronic energies only, while the entropic effects are considered to have only a minor effect on the reaction profiles. This conclusion is supported by a series of test calculations, with the results summarized in Supporting Information.

Over the course of the reaction, $H_2O$ molecules leave the Fe sites and new $H_2O$ molecules are formed (e.g., upon decomposition of $H_2O_2$) that are not connected to the Fe atoms. These molecules form a hydrogen-bond network connecting the O- and H-sites associated with the cluster and the zeolite lattice. These networks can very easily rearrange upon methane adsorption and/or transformation without affecting the electronic properties of the reactive Fe species but influencing the overall energy of the system. As a result, we observed that the barrier heights and reaction energies for elementary steps can be quite substantially affected by the positions of these uncoordinated $H_2O$ [$E$(H-bond in water) = ~20 kJ/mol]. Extensive analysis of the different isomeric structures involved in similar reaction steps shows that this is an artifact of the model. In the actual aqueous medium, these effects would have been counterbalanced by the presence of bulk $H_2O$ molecules. However, the comprehensive sampling required for such an extensive model is in conflict with the goals of the present study. Therefore, we neglected the respective effects and always removed noncoordinated physically adsorbed $H_2O$ molecules from the unit cell after their formation. The resulting desorption energy of $H_2O$ molecules is not discussed in this article, but it is shown in the reaction energy diagrams (e.g., reaction step $2\times H_2O/\mathbf{5} \rightarrow \mathbf{5}$ in Figure 8).

The numbering of structures in the paper is not presented in sequential order but follows individual reaction paths from the beginning to the formation of $CH_3OH$ or $CH_3OOH$ (as summarized in Figures S1 and S2). Conformational isomers and $CH_4$ adsorbed in different positions of the same active site are marked with **v** after structure number. $H_2O$ in front of the structure number indicates an uncoordinated $H_2O$ molecule, which will be removed in a later step of the reaction.

Images of structures were created with Visual Molecular Dynamics (VMD) software.[66,67]

## 3. RESULTS AND DISCUSSION

A schematic representation of the favorable reaction mechanisms identified in our study is shown in Figure 2. Detailed structures can be found in Figures S1 and S2. The active Fe(III) and Fe(IV) sites are formed by adsorption and dissociation of



DOI: 10.1021/acscatal.8b01672
ACS Catal. 2018, 8, 7961−7972

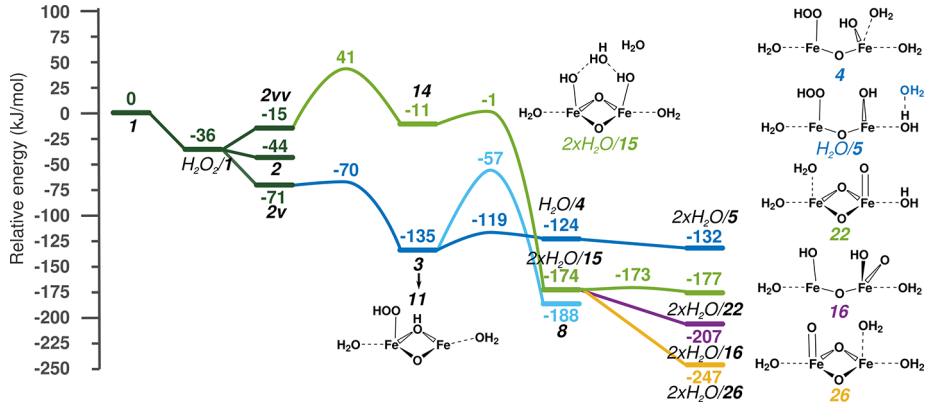


**Figure 3.** Potential reaction pathways for active-site formation via reaction of the Fe cluster with $H_2O_2$ and schematic representations of key intermediates.

$H_2O_2$. Reorganization of the H ions results in different active sites. Our calculations show that Fe(III) species catalyze heterolytic and Fenton-type activation, while Fe(IV) species facilitate homolytic activation of methane. The Fe clusters are grouped on the basis of average formal oxidation state. For example, if one Fe atom is formally +2 while the other is in +4 oxidation state, the average is +3 and the cluster is considered an Fe(III) cluster. The structures of all clusters can be found in Figures S1 and S2.

From Fe(III) species, methanol can be formed via combination of the methyl group and an OH group before or after oxidation of the cluster by the peroxo ligand. In the cases of homolytic and Fenton-type mechanisms, a methyl radical is formed, which can further transform to $CH_3OH$ via a rebound mechanism or to $CH_3OOH$ via reaction with $O_2$ (inevitably formed by a parallel $H_2O_2$ decomposition process) and abstraction of a H atom from the active site. Fe(IV) sites are the active species for both homolytic dissociation of methane and decomposition of $H_2O_2$ to $O_2$ and $[H^+]$ ions. In the following sections, we provide detailed descriptions of each reaction step.

**3.1. Active-Site Formation.** The first step of the reaction is formation of the active site. All investigated pathways (Figure 3) start with adsorption of $H_2O_2$ in the zeolite pore ($H_2O_2$/**1**) and its subsequent coordination to the active site, where it substitutes one $H_2O$ molecule (**2**). These steps are exothermic by −44 kJ/mol. The conformational isomers **2v** and **2vv**, shown in Figure 3, are formed by rotation of the noncoordinated $H_2O$ molecule and $H_2O_2$. The difference in energy between these structures is an artifact of the model, resulting from the rearrangement of H bonds as described in the Model and Simulation Details section. This structural rearrangement is necessary to adequately probe alternative reaction pathways for the subsequent steps involving the $H_2O$ molecule as a proton mediator. From this stage, two alternative reaction channels can be distinguished that result in an active site: namely, (1) direct oxidation of both Fe(III) centers to Fe(IV), via homolytic cleavage of the peroxide moiety, and (2) deprotonation of $H_2O_2$ to form an Fe-bound peroxo ligand, leaving the formal oxidation state of the iron ions unchanged.

The first path proceeds with a barrier of only 56 kJ/mol and yields a transient OH radical (**14**) that readily subtracts a H atom from a neighboring coordinated $H_2O$ ($E^{\#}$ = 10 kJ/mol), resulting in 2×$H_2O$/**15**. The isomerization of this species by proton reshuffling gives 2×$H_2O$/**22** ($\Delta E$ = −3 kJ/mol) and 2×$H_2O$/**26** ($\Delta E$ = −73 kJ/mol). Such a water-assisted H transfer is a very facile reaction that, in the case of the 2×$H_2O$/**15** → 2×$H_2O$/**22** step, shows a barrier of 1 kJ/mol. Since we expect the activation barrier for similar H-bonding rearrangements to be on the same order of magnitude, the transition states were not located in other cases. This type of reaction for ferryl ion formation was considered earlier by Baerends and coworkers.[68,69] An alternative path of 2×$H_2O$/**15** → 2×$H_2O$/**16** leads to the cleavage of one Fe-$\mu$O bond ($\Delta E$ = −33 kJ/mol). The diamond shape of the Fe-oxo cluster transforms to a near-linear Fe−O−Fe species and a terminal O is formed. Transition-state energy was found to be low for this type of reaction, as described in the next paragraph for the reaction **3** → $H_2O$/**4**.

The second path starts with deprotonation of $H_2O_2$ by the bridging O site to form a bridging OH group and a terminal OOH ligand (**3**). The noncoordinating $H_2O$ molecule facilitates this reaction via a proton shuttling mechanism. Next, the Fe−$\mu$OH bond breaks with an activation barrier of only 16 kJ/mol to form an activated intermediate $H_2O$/**4**, which is a near-linear Fe−O−Fe cluster with a terminal OH ligand. This reaction is similar to the previously described 2×$H_2O$/**15** → 2×$H_2O$/**16** transformation. The activation barrier of other Fe−$\mu$O bond cleavage reactions is expected to be in the same range as other similar reactions, and it is significantly lower than that of the rate-determining step; therefore, the activation barriers of similar steps were not calculated for other cases.

In the next reaction step, $H_2O$ is decoordinated from the Fe center. This is necessary because, during the heterolytic dissociation, formation of an Fe−C bond occurs. Since the complex is originally in octahedral coordination, this would not be possible without the removal of one ligand. We decided to decouple $H_2O$ decoordination from $CH_4$ activation because otherwise the energy change resulting from forming H bonds and Fe−O bond breaking would artificially be included in the reaction and the transition-state energies of C−H bond dissociation. In the reaction $H_2O$/**4** → 2×$H_2O$/**5** ($\Delta E$ = 9 kJ/mol), one $H_2O$ molecule leaves the Fe atom. Removal of one $H_2O$ molecule from 2×$H_2O$/**5** results in $H_2O$/**5** (shown in Figure 3), and by removal of the second uncoordinated $H_2O$ molecule, **5** is obtained. In this case the Fe atom where the $H_2O$ was removed from has only five ligands. This will be the Fe atom that will form the Fe−C bond. We are going to focus on this Fe atom further in this paragraph. The removal of two $H_2O$ molecules, one coordinated and one uncoordinated, from **3** results in **11**, which also has a five-coordinated Fe atom. The difference between **11** and **5** is that the Fe in **11** has one ligand that moves freely while the other four, the framework, and the



DOI: 10.1021/acscatal.8b01672
ACS Catal. 2018, 8, 7961−7972

bridging O atoms are in fixed positions. The Fe atom of **5** has two ligands that are rather flexible: an $H_2O$ molecule and an OH ligand. This difference leads to different structures. The Fe atom of **11** is in a square pyramid geometry, while the Fe of **5** is closer to a trigonal bipyramidal geometry.

The first pathway is thermodynamically more favorable than the second, while the second has lower reaction barriers and thus is kinetically more favorable. However, if we inspect the structures more closely, we realize that by cleaving the peroxo bond of **3**(→**8**) ($\Delta E$ = −53 kJ/mol; $E^{\#}$ = 78 kJ/mol) and reshuffling the protons of **8**, the structures of the first pathway can be obtained. This indicates that the occurrence of all previously described structures is feasible.

To decrease the influence of fluctuating H bonds, the $H_2O$ molecules not coordinated to the Fe were removed (vide supra). This way the structures shown in Figure 3—**4**, **5**, **11**, **16**, **22**, and **26**—were obtained. These are the active sites applied in the subsequent C−H bond activation steps. After removal of the extra water molecules, the difference in energy between **15**, **16**, **22**, and **26** decreases from 127 to 23 kJ/mol. Their order of stability also changes: **16** becomes the most stable species among them. This energy difference is rather small. In the next section, we consider the active site and the gas-phase methane for all reactions as reference points to enable direct assessment of their reactivity.

**3.2. C−H Bond Activation.** The next step of the reaction is the C−H bond cleavage of methane. The previously described Fe(III) and Fe(IV) complexes were selected to act as active sites in the reaction. As can be seen in Figure 2, Fe(III) complexes catalyze the heterolytic and Fenton-type reactions while Fe(IV) complexes promote the homolytic oxidation of methane. Figure 4 shows a sample transition state for each case. The isosurface

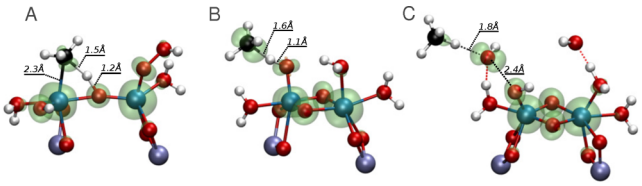


**Figure 4.** Transition states typical for (A) heterolytic dissociation, reaction **5** → **9**; (B) homolytic dissociation, reaction **26** → **27**; and (C) Fenton-type dissociation, reaction **2** → **13**. The isosurface represents the spin density. Color coding: Al, purple; Fe, blue; O, red; C, black; H, white. The clusters shown here are part of a periodic model containing the unit cell of ZSM-5 zeolite, the Fe cluster, and the reactants.

represents the spin density. Figure 4 A is a representative of the heterolytic dissociation (**5** → **9**). The bridging O subtracts H from $CH_4$, and the $CH_3$ ligand is already connected to Fe in the transition state, which means that the Fe orbitals participate in the reaction. The lack of spin density around C indicates that there are no unpaired electrons on the C orbitals, and this is indeed a heterolytic dissociation. Figure 4 B shows the transition state of reaction **26** → **27**, a homolytic C−H bond dissociation. In this case the terminal O accepts the H atom and $CH_3$ radical is formed. The C−H bond distance is smaller than the H−O bond distance, implying a late transition state. This is typical for the terminal O; however, in other type of O atoms (bridging O or OH ligand) this is not necessarily the situation. The spin density isosurface shows that C has more $\alpha$- than $\beta$-electrons, indicative of a radical reaction. Figure 4C shows the transition state of a Fenton-type C−H bond dissociation (**2** → **13**). Spin density accumulates around the forming OH radical, which cleaves the C−H bond. This is also a radical reaction.

In the following subsections we present the detailed cases of each type of $CH_4$ activation.

*3.2.1. Heterolytic Activation.* The reaction energy diagram of heterolytic activation is shown in Figure 5. The reference point is

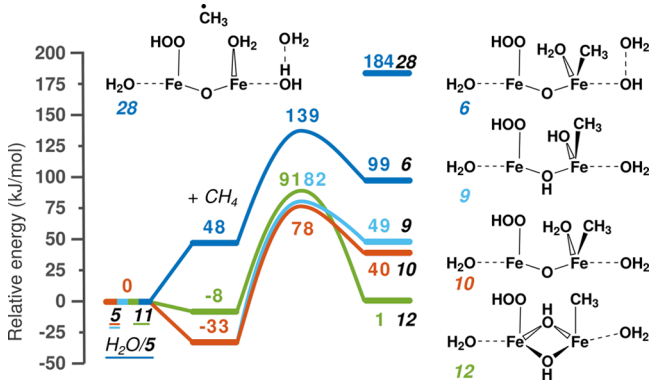


**Figure 5.** Reaction energy diagram of heterolytic C−H bond cleavage of methane. The reference point is the active site and gas-phase methane. The first step is methane adsorption in the zeolite pore, followed by heterolytic dissociation of the first C−H bond of methane and the formation of an Fe−$CH_3$ moiety and an OH ligand or water, depending on the nature of the proton-accepting site.

the active site and gas-phase methane. At first methane is adsorbed in the zeolite pore, which is followed by heterolytic dissociation of the first C−H bond of $CH_4$ and formation of a $CH_3$ group and an OH ligand or $H_2O$. For this reaction to occur, Fe needs to have an empty coordination site to accommodate the $CH_3$ group. Hence one $H_2O$ ligand was decoordinated from one of the Fe atoms during formation of the active site followed by the removal of one or two physically adsorbed $H_2O$ molecules as described in the previous section (2×$H_2O$/**4** → **5** and $H_2O$/**5**; **3** → **11**).

The first possibility is the reaction $H_2O$/**5** → **6** (dark blue). It starts with $CH_4$ adsorption in the zeolite pore. Since the Fe site is not located in the main channel, there is not enough space for the methane to coordinate favorably to the active site. The confinement of the framework and the cluster results in repulsive forces around the methane. This entails a positive adsorption energy and a relatively high reaction energy (99 kJ/mol) and reaction barrier (139 kJ/mol).

Reactions **5** → **9** (light blue) and **5** → **10** (orange) show the reaction over the same cluster as $H_2O$/**5** but with one fewer $H_2O$ molecule around the cluster. Methane is adsorbed at a different position, resulting in a negative adsorption energy. The difference between the two reactions is the activating O. In reaction **5** → **9**, methane is activated by a bridging O ($\Delta E$ = 49 kJ/mol, $E^{\#}$ = 82 kJ/mol), while in reaction **5** → **10**, methane is activated by the terminal OH group ($\Delta E$ = 40 kJ/mol, $E^{\#}$ = 78 kJ/mol). Since both the reaction barrier and energy are very similar, this indicates that the type of O does not influence the reactivity significantly.

Next, we compare the performance of two active sites, **5** and **11**. As described previously, these two structures have an Fe atom with five ligands in different geometries. The comparison of paths **5** → **9** and **11** → **12** shows that this difference in geometry does not have an effect on the reaction barrier (91 vs 82 kJ/mol, respectively); however, formation of the octahedral



DOI: 10.1021/acscatal.8b01672
ACS Catal. 2018, 8, 7961−7972

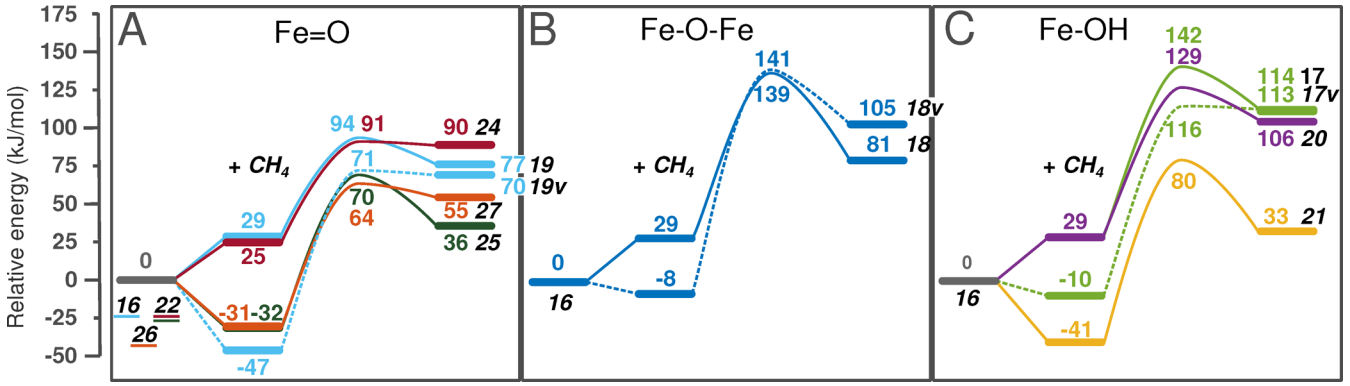


**Figure 6.** Reaction energy diagram of homolytic C−H bond cleavage of methane. The reference point is the active site and gas-phase methane. The first step is methane adsorption in the zeolite pore, followed by homolytic dissociation of the first C−H bond of methane and formation of a methyl radical and an OH ligand or water. The same-colored lines represent reaction pathways where the cluster and the H-accepting oxygen are the same but the position of adsorbed methane is different.

environment greatly stabilizes **12** (reaction energy of 49 vs 1 kJ/mol).

It is interesting to take the adsorbed methane as the reference point for our comparison. The qualitative picture for **5** → **9**, **5** → **10**, and **11** → **12** does not change remarkably. However, reaction $H_2O$/**5** → **6** will have much lower reaction barrier and energy, so that it becomes the most favorable path. When confinement plays a role, the adsorption has to be taken into account.

As mentioned earlier, heterolytic activation occurs on Fe(III) sites. In Figure 5, structure **28** is the result of homolytic dissociation over $H_2O$/**5**. The OH group of **5** accepts a H atom and a $CH_3$ radical is formed. The reaction energy is 85 kJ/mol higher compared to the formation of intermediate **6**, where instead of $CH_3$ radical a $CH_3$ ligand is formed. This is most likely due to the fact that homolytic dissociation entails the reduction of the Fe site, in this case to the Fe(II) state, while there is no formal oxidation state change for heterolytic dissociation.

*3.2.2. Homolytic Activation.* The reaction energy diagrams of homolytic C−H cleavage are shown in Figure 6. Methane is adsorbed in the zeolite, followed by its homolytic dissociation and formation of a $CH_3$ radical and an OH ligand or $H_2O$ connected to Fe. The formal oxidation state of Fe in the active cluster is +4, which means that the high-spin state is $^8/_2$. During the reaction, one Fe is reduced to +3 while C is formally oxidized. The highest possible spin state becomes $^{10}/_2$ [Fe(III)−Fe(IV) and $CH_3$ radical]; however, it can happen that the $CH_3$ radical is antiferromagnetically coupled with the Fe cluster, and the more stable spin state remains $^8/_2$ at the end of this reaction step. Figure 6 summarizes the results obtained for the most stable configurations.

In Figure 6 the reactions are grouped on the basis of the type of O ligand that abstracts the H from $CH_4$: (A) terminal, (B) bridging, or (C) OH group. The lowest reaction barriers over terminal O and OH are similar (for **22** → **27** and **16** → **21**, $E^{\#}$ = 64 and 80 kJ/mol, respectively); however, the reaction barrier over the bridging O is relatively high ($E^{\#}$ = 139 kJ/mol). This is a result of the position of the Fe cluster, which is not located in the main channel but in a somewhat confined position. The bridging O is not easily accessible. The same reaction modeled in a different position in the main channel resulted in lower adsorption (−43 kJ/mol), reaction barrier (69 kJ/mol), and reaction energies (48 kJ/mol), which are comparable to the best values obtained for Fe═O and Fe−OH (transition-state structure shown in Figure S3). In general, this means that Fe═O, Fe−OH, and Fe−$\mu$O−Fe oxygens are all able to activate methane.

The same trend can be observed here as in the case of the heterolytic dissociation. The positive adsorption energy decreases the intrinsic barriers and reaction energies (reference point is the active site with adsorbed methane); however, compared to the original reference point (gas-phase methane and zeolite), the reactions with positive adsorption energy are less exothermic and have higher barriers. This is emphasized by the same-color reaction pathways, which represent routes where the activating O and the Fe cluster are the same but the methane is adsorbed in a different position in the zeolite. An example is the case of **16** → **19** and **16** → **19v** (light blue in Figure 6 A). In the first case methane adsorbs above the cluster with a positive adsorption energy, while in the second case methane adsorbs in the main channel next to the cluster and accesses the terminal O from there. In the first case the intrinsic activation energy is a mere 65 kJ/mol, while in the second case it is 118 kJ/mol; however, if we take the gas-phase methane as reference, the second reaction becomes more favorable with a reaction barrier of 71 kJ/mol (vs 94 kJ/mol).

*3.2.3. Fenton-type Activation.* Fenton-type activation, as described earlier, is a type of homolytic C−H bond dissociation. The important distinction from the previously presented homolytic dissociation is that the role of the transition metal catalyst is to produce the active OH radicals. Here we present two possibilities for this type of reaction, for which reaction energy diagrams shown in Figure 7. The active sites are **2** and **4**,

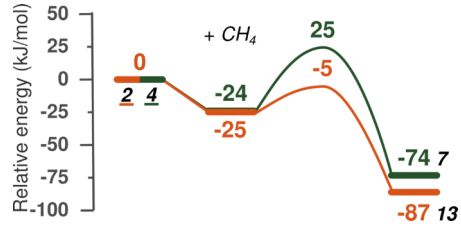


**Figure 7.** Reaction energy diagram of Fenton-type C−H bond cleavage of methane. The reference point is the active site and gas-phase methane. The first step is methane adsorption in the zeolite pore, followed by homolytic dissociation of the peroxo bond, formation of OH radical, and dissociation of the first C−H bond of methane, and then formation of a methyl radical and water molecule in the same step.



DOI: 10.1021/acscatal.8b01672
ACS Catal. 2018, 8, 7961−7972

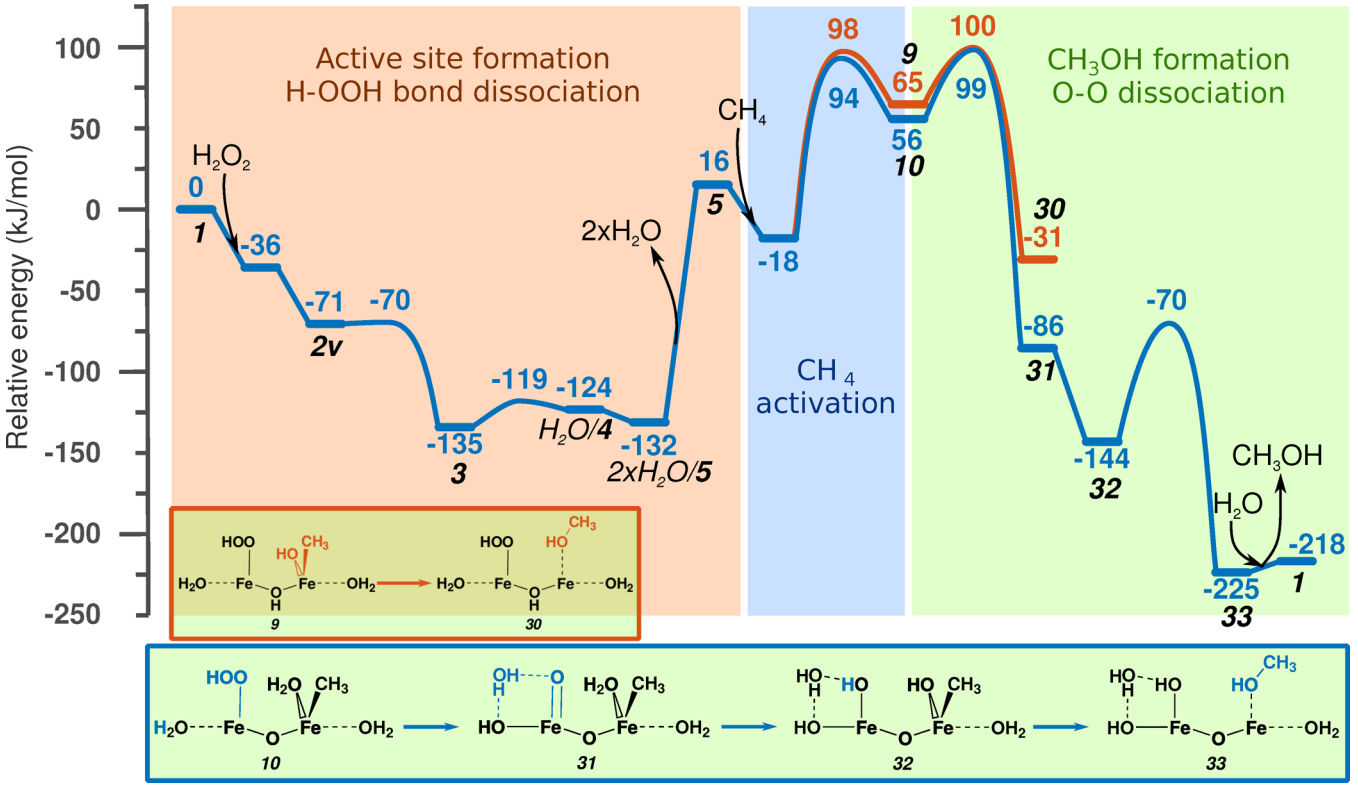


**Figure 8.** Reaction energy diagram of methane to methanol formation, including formation of the active site, heterolytic C−H bond activation, formation of $CH_3OH$, and active-site regeneration.

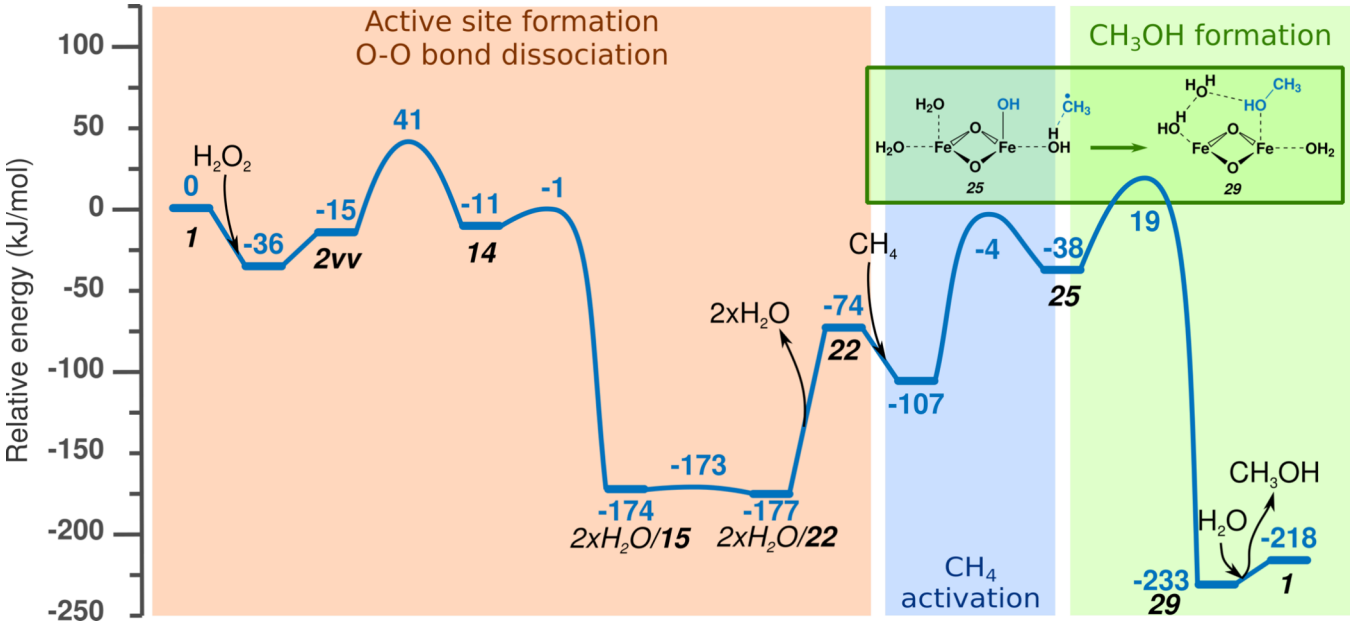


**Figure 9.** Reaction energy diagram of methane to methanol formation, including formation of the active site, homolytic C−H bond activation, formation of $CH_3OH$, and active-site regeneration.

already introduced in the previous section; **2** is formed by coordination of $H_2O_2$ to Fe, while **4** is formed by deprotonation of **2** and consecutive cleavage of the Fe−$\mu$OH group (Figure 3). In the transition states, the $CH_4$ is effectively intact and an OH radical is formed. The reaction can be viewed as a redox reaction, in which the O atoms of $H_2O_2$ oxidize C in methane and Fe of the active site. The reaction yields $CH_3$ radical, $H_2O$ molecule, and Fe(IV)Fe(III) complex. The Fenton-type methane activation is a highly favorable process ($\Delta E$ = −74 and −87 kJ/mol), proceeding with barriers of 25 and −5 kJ/mol (Figure 7).

The lowest activation energy and thermodynamic favorability belongs to the Fenton-type activation. In general, Fenton-type reaction is undesired, because it is very difficult to control and this path is thought to decrease the selectivity of the overall process. The lowest reaction and activation energies of the



DOI: 10.1021/acscatal.8b01672
ACS Catal. 2018, 8, 7961−7972

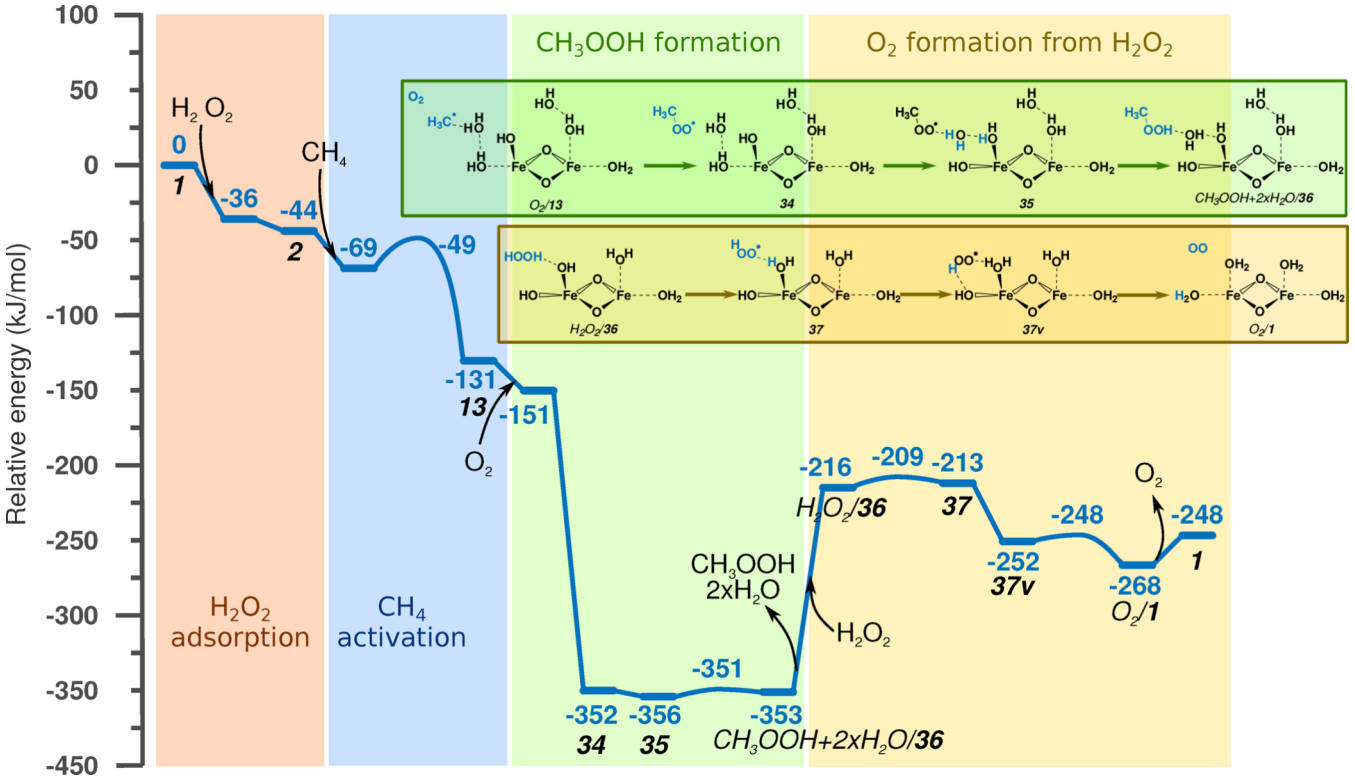


**Figure 10.** Reaction energy diagram of methane to $CH_3OOH$ formation, including formation of the active site, Fenton-type C−H bond activation, formation of $CH_3OOH$, and active-site regeneration by $H_2O_2$ decomposition to $O_2$.

heterolytic and homolytic dissociation pathways are comparable, which implies that both mechanisms are effectively possible, and all type of O ligands can potentially act as H acceptors, providing a favorable reaction channel for $CH_4$ activation.

**3.3. Closing the Reaction Cycle.** *3.3.1. Methanol Formation after Heterolytic Methane Activation.* The heterolytic mechanism of C−H activation is seldom considered for the selective oxidation process, because the subsequent $CH_3OH$ formation would require a dual-site reductive elimination process. Figure 8 shows the full catalytic cycle through intermediates **10** and **9**. It starts with activation of the binuclear Fe(III) site by $H_2O_2$ to obtain the $2\times H_2O$/**5** active site. The physically adsorbed water is then removed, as explained in the Model and Simulation Details section. This step results in a 148 kJ/mol energy loss of the model system. This is an artificial increase in the overall energy; however, it is necessary to show it here to keep the reference point constant throughout the reaction energy diagram. The same is true for the reaction step $2\times H_2O$/**22** → **22** in Figure 9. The desorption step is followed by adsorption and heterolytic dissociation of $CH_4$. To form methanol, recombination of $CH_3$ and an OH ligand is needed. This decreases the formal oxidation state of Fe(III)Fe(III) by 2, resulting in an Fe(II)Fe(II) structure. This is shown by the orange line in Figure 8, where **9** is transformed to **30** with a barrier of 35 kJ/mol and −96 kJ/mol reaction energy. To regenerate the catalyst, dissociation of the peroxo bond and rearrangement of H ions are needed. These steps are not calculated here; previous calculations indicate that the peroxo bond dissociation proceeds with a barrier of ∼40−70 kJ/mol, and the H atom transfer is almost barrierless.

The other possibility is oxidation of the cluster prior to formation of MeOH. This route is indicated by a blue line in Figure 8. The activation barrier for peroxo bond (**10** → **31**) cleavage is 44 kJ/mol. H atom transfer to form **32** provides a 58 kJ/mol energy gain, which can be explained by the formation of an Fe(IV)Fe(IV) cluster from a formally Fe(V)Fe(III) intermediate. In the next step, MeOH is formed (**33**) with a barrier of 74 kJ/mol that is needed to reduce the Fe atoms. After desorption of MeOH, rearrangement of H atoms, and formation of a bridging O, regeneration of the initial Fe(III)−oxo cluster takes place. As described earlier, all these steps proceed with a low reaction barrier.

These data suggest that there is no energetic preference in the order of MeOH formation and oxidation of the Fe cluster defined.

*3.3.2. Methanol Formation after Homolytic and Fenton-type Activation.* The structures obtained after both homolytic and Fenton-type pathways are similar in nature: they contain a $CH_3$ radical and an Fe(III)Fe(IV) cluster. Figure 9 shows the formation of methanol from **25**, which is the result of combining the $CH_3$ radical with an OH group of the Fe cluster. The reaction step requires 57 kJ/mol activation energy, and it has a reaction energy of −195 kJ/mol. With the substitution of methanol by one water molecule, we obtain the initial structure **1**.

*3.3.3. Methyl Hydroperoxide Formation and $H_2O_2$ Decomposition.* If $CH_3$ radicals are present in the liquid phase, formation of MeOOH is also possible. A potential pathway is illustrated in Figure 10. $CH_3OOH$ formation starts with **13**, where a $CH_3$ radical is formed via Fenton-type homolytic dissociation of methane. The first step of the reaction is adsorption of $O_2$ in the zeolite. $O_2$ is present in water, and it is also formed during the side reaction of $H_2O_2$ decomposition to $H_2O$ and $O_2$. $O_2$ and $CH_3$ radical favorably combine to form an MeOO radical (**34**) with an energy gain of −201 kJ/mol. In the next step, there is H transfer between the Fe−OH and Fe−$OH_2$



DOI: 10.1021/acscatal.8b01672
ACS Catal. 2018, 8, 7961−7972

ligands (**35**) for the H atoms to get into more favorable position for the water-assisted H transfer to MeOO to yield MeOOH ($CH_3OOH + 2\times H_2O$/**36**). As expected, this reaction has an activation barrier of only a few kilojoules per mole and is thermodynamically neutral. Compared to MeOH, the formation of MeOOH is thermodynamically similar: $\Delta E(O_2$/**13** → $CH_3OOH + 2\times H_2O$/**36**) = −202 kJ/mol vs $\Delta E$(**25** → **29**) = −195 kJ/mol. The limiting factor is the $O_2$ concentration in solution compared to the Fe−OH groups or framework O atoms close to the sites of formation of $CH_3$ radicals.

To regenerate the initial site, complex **36** needs to be reduced. There are two reducing agents in the system: $CH_4$ and $H_2O_2$. This means that the active site might cleave a second C−H bond or oxidize $H_2O_2$ to two $[H^+]$ ions and an $O_2$ molecule. The latter option is illustrated in Figure 10. Starting from $CH_3OOH + 2\times H_2O$/**36**, MeOOH and two uncoordinated $H_2O$ molecules are desorbed, and $H_2O_2$ is adsorbed. The first step is abstraction of one H atom from the $H_2O_2$ molecule and formation of an OOH radical (**37**). The second H atom is then abstracted after the rearrangement of the OOH radical, which comes with −39 kJ/mol energy gain due to the formation of a H-bonding interaction (**37v**). The reaction yields the initial site ($O_2$/**1**). The total reaction energy of $O_2$ formation from $H_2O_2$ is −52 kJ/mol, and the activation barrier of both H atom abstractions is less than 10 kJ/mol.

Both $H_2O_2 \rightarrow O_2 + 2[H^+]$ and $CH_4 \rightarrow CH_3 + [H]$ reactions occur on the same Fe(IV)−oxo species. This means that $H_2O_2$ and $CH_4$ are competing for the same sites. Since the activation barrier of $H_2O_2$ oxidation is significantly lower than the barrier of C−H bond dissociation, and usually $H_2O_2$ concentration is significantly higher than that of methane, the dissociation of $H_2O_2$ will be favored over methane. This renders the usage of $H_2O_2$ impractical for methane activation in combination with high-valent Fe−oxo catalysts.

The total reaction energies of methanol and methyl hydroperoxide formation in Figures 8−10 are not directly comparable, due to removal of the physically adsorbed $H_2O$ molecules in Figures 8 and 9 and the adsorption of $O_2$ in Figure 10. We can, however, make an estimation, for example, from Figure 9 by subtracting the desorption energy of the previously removed $H_2O$ molecules ($\Delta E$ = 103 kJ/mol) and adding the adsorption energy of $O_2$ ($\Delta E$ = −20 kJ/mol). This gives $\Delta E$(**1** → $2\times H_2O + O_2$/**29**) ≈ −233 − 123 = −336 kJ/mol, which is comparable to the reaction energy for the alternative reaction channel $\Delta E$(**1** → $CH_3OOH + 2\times H_2O$/**36**) = −353 kJ/mol. However, the calculations indicate that the formation of MeOOH is kinetically more favorable than the formation of MeOH (following Fenton-type or homolytic C−H bond dissociation), as the direct rebound of $CH_3$ radical with an OH group proceeds with a barrier of $E^{\#} \sim 60$ kJ/mol, while recombination of the $CH_3$ radical with an $O_2$ molecule is a barrierless reaction and the only barrier on the path to methyl hydroperoxide is associated with H atom abstraction, which our calculations predict to be very small ($E^{\#}$ = 5 kJ/mol). Comparison with experimental data is difficult, due to the complexity of the reaction network and the potential decomposition of MeOOH to MeOH[16] and to $H_2CO$,[47] and in situ analysis of the reaction mixture is not available. A batch reaction study performed by Hutchings and co-workers[16] shows that, at the beginning of the reaction, selectivity toward MeOOH is high (~60%), and it gradually decreases during the course of the reaction. This supports the kinetic preference for MeOOH formation over MeOH.

## 4. CONCLUSIONS

Different reaction paths for selective methane oxidation over a binuclear Fe site deposited in ZSM-5 zeolite were studied by periodic DFT calculations. The whole reaction cycle was investigated, including formation of the active site, $CH_4$ activation, product formation, and regeneration of the initial site. Special attention was given to the rate-determining C−H bond dissociation step, the possibility of multiple mechanisms, and the influence of different active sites on them. These mechanisms were (1) heterolytic, (2) homolytic and (3) Fenton-type activation.

This study demonstrates that the system cannot be reduced to a single-site single-cycle concept. Even with the simplification to a single type of Fe cluster at a given position of the zeolite framework, the formation of multiple types of active sites is possible, catalyzing three mechanistically different C−H bond activations.

The possibility of formation of different Fe(III) and Fe(IV) clusters upon reaction with $H_2O_2$ was demonstrated. These sites were proven to be catalytically active. Fe(III) was established to promote heterolytic and Fenton-type reactions, while Fe(IV) was shown to promote the homolytic reaction.

We found that the geometry of the Fe complex significantly influences the reaction energy but not the barrier of heterolytic C−H bond activation. The calculations indicate that the type of activating O (Fe═O, Fe−$\mu$O−Fe, or Fe−OH) is unimportant from an energetic point of view for both types of activation. We also found that confinement of the zeolite has a significant effect on the reaction step.

Methanol can be formed following all types of C−H bond activation via recombination of $CH_3$ and an OH ligand reducing the active site. If the C−H bond was previously heterolytically cleaved, this step can either precede or follow oxidation of the active site by peroxo bond cleavage. After homolytic and Fenton-type dissociation, this reduction step restores the initial oxidation state of the active site. MeOOH can be obtained from the reaction of $CH_3$ radical and $O_2$ molecule, followed by abstraction of a H atom from the active site. After this step, the Fe site is in the oxidized form available for further $CH_4$ oxidation.

Since the reaction is accompanied by excessive consumption of $H_2O_2$, its decomposition was also investigated. We found that the same Fe(IV)−oxo sites promote the oxidation of both $H_2O_2$ and $CH_4$. The first reaction will be dominant, as the activation barrier for O−H bond cleavage is significantly lower than for C−H bond cleavage. This is why we propose $H_2O_2$ to be an unsuitable oxidant in combination with high-valent Fe clusters.

## ■ ASSOCIATED CONTENT

### Supporting Information

The Supporting Information is available free of charge on the ACS Publications website at DOI: 10.1021/acscatal.8b01672.

Seven figures showing schematic representations of reaction pathways, TS structure, and reaction energy diagrams; additional text describing free energy calculation; and coordinates of all calculated stable point and transition-state structures in the most stable spin state (PDF)

## ■ AUTHOR INFORMATION

### Corresponding Author

*E-mail e.a.pidko@tudelft.nl; phone +31 1527 81938.



DOI: 10.1021/acscatal.8b01672
ACS Catal. 2018, 8, 7961−7972

**ORCID**

Guanna Li: 0000-0003-3031-8119
Jorge Gascon: 0000-0001-7558-7123
Evgeny A. Pidko: 0000-0001-9242-9901

**Notes**

The authors declare no competing financial interest.

## ■ ACKNOWLEDGMENTS

We thank Elena Khramenkova (ITMO University) for carrying out some of the calculations. The Dutch Science Foundation (NWO) is gratefully acknowledged for financial support through the VIDI personal grant MetMOFCat. G.L. acknowledges financial support from NWO for her personal VENI grant (016.Veni.172.034). E.A.P. acknowledges partial support from the Ministry of Education and Science of the Russian Federation (Project 11.1706.2017/4.6). SurfSARA and NWO (The Netherlands Organisation for Scientific Research) are acknowledged for providing access to supercomputer resources.

## ■ REFERENCES

(1) Arndtsen, B. A.; Bergman, R. G.; Mobley, T. A.; Peterson, T. H. Selective Intermolecular Carbon-Hydrogen Bond Activation by Synthetic Metal Complexes in Homogeneous Solution. *Acc. Chem. Res.* **1995**, *28*, 154−162.

(2) Bergman, R. G. Organometallic Chemistry: C-H Activation. *Nature* **2007**, *446*, 391−393.

(3) Olivos-Suarez, A. I.; Szécsényi, A.; Hensen, E. J. M.; Ruiz-Martinez, J.; Pidko, E. A.; Gascon, J. Strategies for the Direct Catalytic Valorization of Methane Using Heterogeneous Catalysis: Challenges and Opportunities. *ACS Catal.* **2016**, *6*, 2965−2981.

(4) Edwards, J. H.; Foster, N. R. The Potential for Methanol Production from Natural Gas by Direct Catalytic Partial Oxidation. *Fuel Sci. Technol. Int.* **1986**, *4*, 365−390.

(5) Zhang, Q.; He, D.; Zhu, Q. Recent Progress in Direct Partial Oxidation of Methane to Methanol. *J. Nat. Gas Chem.* **2003**, *12*, 81−89.

(6) Ravi, M.; Ranocchiari, M.; van Bokhoven, J. A. The Direct Catalytic Oxidation of Methane to Methanol-A Critical Assessment. *Angew. Chem., Int. Ed.* **2017**, *56*, 16464−16483.

(7) Parkyns, N. D.; Warburton, C. I.; Wilson, J. D. Natural Gas Conversion to Liquid Fuels and Chemicals: Where Does It Stand? *Catal. Today* **1993**, *18*, 385−442.

(8) Hammond, C.; Conrad, S.; Hermans, I. Oxidative Methane Upgrading. *ChemSusChem* **2012**, *5*, 1668−1686.

(9) Bone, W. A.; Wheeler, R. V. LVIII. - The Slow Oxidation of Methane at Low Temperatures. *J. Chem. Soc., Trans.* **1902**, *81*, 535−549.

(10) Periana, R.; Taube, D.; Evitt, E.; Löffler, D.; Wentrcek, P.; Voss, G.; Masuda, T. A Mercury-Catalyzed, High-Yield System for the Oxidation of Methane to Methanol. *Science* **1993**, *259*, 340−343.

(11) Periana, R.; Taube, D.; Gamble, S.; Taube, H.; Satoh, T.; Fujii, H. Platinum Catalysts for The High-Yield Oxidation of Methane to a Methanol Derivative. *Science* **1998**, *280*, 560−564.

(12) Groothaert, M. H.; Smeets, P. J.; Sels, B. F.; Jacobs, P. A.; Schoonheydt, R. A. Selective Oxidation of Methane by the Bis(μ-oxo)dicopper Core Stabilized on ZSM-5 and Mordenite Zeolites. *J. Am. Chem. Soc.* **2005**, *127*, 1394−1395.

(13) Beznis, N. V.; Weckhuysen, B. M.; Bitter, J. H. Partial Oxidation of Methane over Co-ZSM-5: Tuning the Oxygenate Selectivity by Altering the Preparation Route. *Catal. Lett.* **2010**, *136*, 52−56.

(14) Shan, J.; Huang, W.; Nguyen, L.; Yu, Y.; Zhang, S.; Li, Y.; Frenkel, A. I.; Tao, F. Conversion of Methane to Methanol with a Bent Mono(μ-oxo)Dinickel Anchored on the Internal Surfaces of Micropores. *Langmuir* **2014**, *30*, 8558−8569.

(15) Xu, J.; Zheng, A.; Wang, X.; Qi, G.; Su, J.; Du, J.; Gan, Z.; Wu, J.; Wang, W.; Deng, F. Room Temperature activation of Methane over Zn Modified H-ZSM-5 Zeolites: Insight from Solid-State NMR and Theoretical Calculations. *Chem. Sci.* **2012**, *3*, 2932−2940.

(16) Hammond, C.; Forde, M. M.; Ab Rahim, M. H.; Thetford, A.; He, Q.; Jenkins, R. L.; Dimitratos, N.; Lopez-Sanchez, J. A.; Dummer, N. F.; Murphy, D. M.; Carley, A. F.; Taylor, S. H.; Willock, D. J.; Stangland, E. E.; Kang, J.; Hagen, H.; Kiely, C. J.; Hutchings, G. J. Direct Catalytic Conversion of Methane to Methanol in an Aqueous Medium by Using Copper-Promoted Fe-ZSM-5. *Angew. Chem., Int. Ed.* **2012**, *51*, 5129−5133.

(17) Hammond, C.; Dimitratos, N.; Lopez-Sanchez, J. A.; Jenkins, R. L.; Whiting, G.; Kondrat, S. A.; Ab Rahim, M. H.; Forde, M. M.; Thetford, A.; Hagen, H.; Stangland, E. E.; Moulijn, J. M.; Taylor, S. H.; Willock, D. J.; Hutchings, G. J. Aqueous-Phase Methane Oxidation over Fe-MFI Zeolites; Promotion Through Isomorphous Framework Substitution. *ACS Catal.* **2013**, *3*, 1835−1844.

(18) Sobolev, V. I.; Dubkov, K. A.; Panna, O. V.; Panov, G. I. Selective Oxidation of Methane to Methanol on a FeZSM-5 Surface. *Catal. Today* **1995**, *24*, 251−252.

(19) Parfenov, M. V.; Starokon, E. V.; Pirutko, L. V.; Panov, G. I. Quasicatalytic and Catalytic Oxidation of Methane to Methanol by Nitrous Oxide over FeZSM-5 Zeolite. *J. Catal.* **2014**, *318*, 14−21.

(20) Kulkarni, A. R.; Zhao, Z.-J.; Siahrostami, S.; Nørskov, J. K.; Studt, F. Cation-Exchanged Zeolites for the Selective Oxidation of Methane to Methanol. *Catal. Sci. Technol.* **2018**, *8*, 114−123.

(21) Narsimhan, K.; Iyoki, K.; Dinh, K.; Román-Leshkov, Y. Catalytic Oxidation of Methane into Methanol over Copper-Exchanged Zeolites with Oxygen at Low Temperature. *ACS Cent. Sci.* **2016**, *2*, 424−429.

(22) Hammond, C.; Jenkins, R. L.; Dimitratos, N.; Lopez-Sanchez, J. A.; Ab Rahim, M. H.; Forde, M. M.; Thetford, A.; Murphy, D. M.; Hagen, H.; Stangland, E. E.; Moulijn, J. M.; Taylor, S. H.; Willock, D. J.; Hutchings, G. J. Catalytic and Mechanistic Insights of the Low-Temperature Selective Oxidation of Methane over Cu-Promoted Fe-ZSM-5. *Chem. - Eur. J.* **2012**, *18*, 15735−15745.

(23) Hammond, C.; Dimitratos, N.; Jenkins, R. L.; Lopez-Sanchez, J. A.; Kondrat, S. A.; Hasbi Ab Rahim, M.; Forde, M. M.; Thetford, A.; Taylor, S. H.; Hagen, H.; Stangland, E. E.; Kang, J. H.; Moulijn, J. M.; Willock, D. J.; Hutchings, G. J. Elucidation and Evolution of the Active Component within Cu/Fe/ZSM-5 for Catalytic Methane Oxidation: From Synthesis to Catalysis. *ACS Catal.* **2013**, *3*, 689−699.

(24) Hammond, C.; Hermans, I.; Dimitratos, N. Biomimetic Oxidation with Fe-ZSM-5 and $H_2O_2$ - Identification of an Active, Extra-Framework Binuclear Core and an FeIII-OOH Intermediate with Resonance-Enhanced Raman Spectroscopy. *ChemCatChem* **2015**, *7*, 434−440.

(25) Boudart, M. Catalysis by Supported Metals. *Adv. Catal.* **1969**, *20*, 153−166.

(26) Boudart, M.; McDonald, M. A. Structure Sensitivity of Hydrocarbon Synthesis from CO and $H_2$. *J. Phys. Chem.* **1984**, *88*, 2185−2195.

(27) Hargreaves, J. S. J.; Hutchings, G. J.; Joyner, R. W.; Kiely, C. J. The Relationship Between Catalyst Morphology and Performance in the Oxidative Coupling of Methane. *J. Catal.* **1992**, *135*, 576−595.

(28) Meher, S. K.; Ranga Rao, G. Tuning, via Counter Anions, the Morphology and Catalytic Activity of $CeO_2$ Prepared under Mild Conditions. *J. Colloid Interface Sci.* **2012**, *373*, 46−56.

(29) Lv, P.; Lu, Z.; Li, S.; Ma, D.; Zhang, W.; Zhang, Y.; Yang, Z. Tuning Metal Cluster Catalytic Activity with Morphology and Composition: A DFT Study of $O_2$ Dissociation at the Global Minimum of $Pt_mPd_n$ (m + n = 5) Clusters. *RSC Adv.* **2016**, *6*, 104388−104397.

(30) Li, G.; Vassilev, P.; Sanchez-Sanchez, M.; Lercher, J.; Hensen, E. J. M.; Pidko, E. A. Stability and Reactivity of Copper Oxo-Clusters in ZSM-5 Zeolite for Selective Methane Oxidation to Methanol. *J. Catal.* **2016**, *338*, 305−312.

(31) Snyder, B. E. R.; Vanelderen, P.; Bols, M. L.; Hallaert, S. D.; Böttger, L. H.; Ungur, L.; Pierloot, K.; Schoonheydt, R. A.; Sels, B. F.; Solomon, E. I. The Active Site of Low-Temperature Methane Hydroxylation in Iron-Containing Zeolites. *Nature* **2016**, *536*, 317−321.



DOI: 10.1021/acscatal.8b01672
*ACS Catal.* 2018, 8, 7961−7972

(32) Snyder, B. E. R.; Böttger, L. H.; Bols, M. L.; Yan, J. J.; Rhoda, H. M.; Jacobs, A. B.; Hu, M. Y.; Zhao, J.; Alp, E. E.; Hedman, B.; Hodgson, K. O.; Schoonheydt, R. A.; Sels, B. F.; Solomon, E. I. Structural Characterization of a Non-Heme Iron Active Site in Zeolites That Hydroxylates Methane. *Proc. Natl. Acad. Sci. U. S. A.* **2018**, *115*, 4565−4570.
(33) Li, G.; Pidko, E. A.; Van Santen, R. A.; Feng, Z.; Li, C.; Hensen, E. J. M. Stability and Reactivity of Active Sites for Direct Benzene Oxidation to Phenol in Fe/ZSM-5: A Comprehensive Periodic DFT Study. *J. Catal.* **2011**, *284*, 194−206.
(34) Li, G.; Pidko, E. A.; Van Santen, R. A.; Li, C.; Hensen, E. J. M. Stability of Extraframework Iron-Containing Complexes in ZSM-5 Zeolite. *J. Phys. Chem. C* **2013**, *117*, 413−426.
(35) Latimer, A. A.; Kulkarni, A. R.; Aljama, H.; Montoya, J. H.; Yoo, J. S.; Tsai, C.; Abild-Pedersen, F.; Studt, F.; Nørskov, J. K. Understanding Trends in C-H Bond Activation in Heterogeneous Catalysis. *Nat. Mater.* **2017**, *16*, 225−229.
(36) Mahyuddin, M. H.; Tanaka, T.; Shiota, Y.; Staykov, A.; Yoshizawa, K. Methane Partial Oxidation over $[Cu_2(\mu\text{-}O)]^{2+}$ and $[Cu_3(\mu\text{-}O)_3]^{2+}$ Active Species in Large-Pore Zeolites. *ACS Catal.* **2018**, *8*, 1500−1509.
(37) McMullin, C. L.; Pierpont, A. W.; Cundari, T. R. Complete Methane-to-Methanol Catalytic Cycle: A DFT Study of Oxygen Atom Transfer from $N_2O$ to Late-Row (MNi, Cu, Zn) $\beta$-diketiminate CH Activation Catalysts. *Polyhedron* **2013**, *52*, 945−956.
(38) Arvidsson, A. A.; Zhdanov, V. P.; Carlsson, P. A.; Grönbeck, H.; Hellman, A. Metal Dimer Sites in ZSM-5 Zeolite for Methane-to-Methanol Conversion from First-Principles Kinetic Modelling: Is the $[Cu\text{-}O\text{-}Cu]^{2+}$ Motif Relevant for Ni, Co, Fe, Ag, and Au? *Catal. Sci. Technol.* **2017**, *7*, 1470−1477.
(39) Shilov, A. E.; Shul'pin, G. B. Activation of C-H Bonds by Metal Complexes. *Chem. Rev.* **1997**, *97*, 2879−2932.
(40) Copéret, C. C-H Bond Activation and Organometallic Intermediates on Isolated Metal Centers on Oxide Surfaces. *Chem. Rev.* **2010**, *110*, 656−680.
(41) Mayer, J. M. Understanding Hydrogen Atom Transfer: From Bond Strengths to Marcus Theory. *Acc. Chem. Res.* **2011**, *44*, 36−46.
(42) Aljama, H.; Nørskov, J. K.; Abild-Pedersen, F. Theoretical Insights into Methane C-H Bond Activation on Alkaline Metal Oxides. *J. Phys. Chem. C* **2017**, *121*, 16440−16446.
(43) Plietker, B., Ed. *Iron Catalysis: Fundamentals and Applications*; Wiley−VCH: Weinheim, Germany, 2008; DOI: 10.1007/978-3-642-14670-1.
(44) Pignatello, J. J.; Oliveros, E.; MacKay, A. *Crit. Rev. Environ. Sci. Technol.* **2006**, *36*, 1−84.
(45) Pestovsky, O.; Stoian, S.; Bominaar, E. L.; Shan, X.; Münck, E.; Que, L., Jr.; Bakac, A. Aqueous FeIV = O: Spectroscopic Identification and Oxo-Group Exchange. *Angew. Chem., Int. Ed.* **2005**, *44*, 6871−6874.
(46) Shulpin, G. B.; Nizova, G. V. Formation of Alkyl Peroxides in Oxidation of Alkanes by $H_2O_2$ Catalyzed by Transition Metal Complexes. *React. Kinet. Catal. Lett.* **1992**, *48*, 333−338.
(47) Nizova, G. V.; Süss-Fink, G.; Shul'pin, G. B. Catalytic Oxidation of Methane to Methyl Hydroperoxide and Other Oxygenates under Mild Conditions. *Chem. Commun.* **1997**, 397−398.
(48) Süss-Fink, G.; Nizova, G. V.; Stanislas, S.; Shul'Pin, G. B. Oxidations by the Reagent '$O_2$-$H_2O_2$ - Vanadate Anion - Pyrazine- 2-Carboxylic Acid'. Part 10. Oxygenation of Methane in Acetonitrile and Water. *J. Mol. Catal. A: Chem.* **1998**, *130*, 163−170.
(49) Agarwal, N.; Freakley, S. J.; McVicker, R. U.; Althahban, S. M.; Dimitratos, N.; He, Q.; Morgan, D. J.; Jenkins, R. L.; Willock, D. J.; Taylor, S. H.; Kiely, C. J.; Hutchings, G. J. Aqueous Au-Pd Colloids Catalyze Selective $CH_4$ Oxidation to $CH_3OH$ with $O_2$ under Mild Conditions. *Science* **2017**, *358*, 223−227.
(50) Yoshizawa, K.; Shiota, Y.; Yumura, T.; Yamabe, T. Direct Methane-Methanol and Benzene-Phenol Conversions on Fe-ZSM-5 Zeolite: Theoretical Predictions on the Reaction Pathways and Energetics. *J. Phys. Chem. B* **2000**, *104*, 734−740.
(51) Fellah, M. F.; Onal, I. Direct Methane Oxidation to Methanol by $N_2O$ on Fe- and Co-ZSM-5 Clusters with and without Water: A Density Functional Theory Study. *J. Phys. Chem. C* **2010**, *114*, 3042−3051.
(52) Montejo-Valencia, B. D.; Pagán-Torres, Y. J.; Martínez-Iñesta, M. M.; Curet-Arana, M. C. Density Functional Theory (DFT) Study to Unravel the Catalytic Properties of M-Exchanged MFI, (M = Be, Co, Cu, Mg, Mn, Zn) for the Conversion of Methane and Carbon Dioxide to Acetic Acid. *ACS Catal.* **2017**, *7*, 6719−6728.
(53) Kresse, G.; Hafner, J. *Ab initio* Molecular Dynamics for Liquid Metals. *Phys. Rev. B: Condens. Matter Mater. Phys.* **1993**, *47*, 558−561.
(54) Kresse, G.; Hafner, J. *Ab initio* Molecular-Dynamics Simulation of the Liquid-Metalamorphous- Semiconductor Transition in Germanium. *Phys. Rev. B: Condens. Matter Mater. Phys.* **1994**, *49*, 14251−14269.
(55) Kresse, G.; Furthmüller, J. Efficient Iterative Schemes for *ab initio* Total-Energy Calculations Using a Plane-Wave Basis Set. *Phys. Rev. B: Condens. Matter Mater. Phys.* **1996**, *54*, 11169−11186.
(56) Kresse, G.; Furthmüller, J. Efficiency of *ab-initio* Total Energy Calculations for Metals and Semiconductors Using a Plane-Wave Basis Set. *Comput. Mater. Sci.* **1996**, *6*, 15−50.
(57) Perdew, J. P.; Burke, K.; Ernzerhof, M. Generalized Gradient Approximation Made Simple. *Phys. Rev. Lett.* **1996**, *77*, 3865−3868.
(58) Perdew, J. P.; Burke, K.; Ernzerhof, M. Erratum: Generalized Gradient Approximation Made Simple (Physical Review Letters (1996) 77 (3865)). *Phys. Rev. Lett.* **1997**, *78*, 1396.
(59) Blöchl, P. Projector Augmented-Wave Method. *Phys. Rev. B: Condens. Matter Mater. Phys.* **1994**, *50*, 17953−17979.
(60) Kresse, G.; Joubert, D. From Ultrasoft Pseudopotentials to the Projector Augmented-Wave Method. *Phys. Rev. B: Condens. Matter Mater. Phys.* **1999**, *59*, 1758−1775.
(61) Grimme, S.; Antony, J.; Ehrlich, S.; Krieg, H. *J. Chem. Phys.* **2010**, *132*, 154104.
(62) Monkhorst, H. J.; Pack, J. D. Special Points for Brillouin-Zone Integrations. *Phys. Rev. B* **1976**, *13*, 5188−5192.
(63) Mills, G.; Jónsson, H.; Schenter, G. K. Reversible Work Transition State Theory: Application to Dissociative Adsorption of Hydrogen. *Surf. Sci.* **1995**, *324*, 305−337.
(64) Hansen, N.; Heyden, A.; Bell, A. T.; Keil, F. J. A Reaction Mechanism for the Nitrous Oxide Decomposition on Binuclear Oxygen Bridged Iron Sites in Fe-ZSM-5. *J. Phys. Chem. C* **2007**, *111*, 2092−2101.
(65) Belanzoni, P.; Bernasconi, L.; Baerends, E. J. $O_2$ Activation in a Dinuclear Fe(II)/EDTA Complex: Spin Surface Crossing as a Route to Highly Reactive Fe(IV)oxo Species. *J. Phys. Chem. A* **2009**, *113*, 11926−11937.
(66) Humphrey, W.; Dalke, A.; Schulten, K. VMD - Visual Molecular Dynamics. *J. Mol. Graphics* **1996**, *14*, 33−38.
(67) Stone, J. An Efficient Library for Parallel Ray Tracing and Animation. M.Sc. thesis, Computer Science Department, University of Missouri—Rolla, 1998.
(68) Ensing, B., Jr.; Buda, F.; Blöchl, P.; Baerends, E. J. Chemical Involvement of Solvent Water Molecules in Elementary Steps of the Fenton Oxidation Reaction. *Angew. Chem., Int. Ed.* **2001**, *40*, 2893−2895.
(69) Buda, F.; Ensing, B.; Gribnau, M. C. M.; Baerends, E. J. DFT Study of the Active Intermediate in the Fenton Reaction. *Chem. - Eur. J.* **2001**, *7*, 2775−2783.


DOI: 10.1021/acscatal.8b01672
*ACS Catal.* 2018, 8, 7961−7972